ISTITUTO NAZIONALE DI FISICA NUCLEARE

Sezione di Torino

INFN/TC-83/2
24 Gennaio 1983

C. Manfredotti and U. Nastasi: A MONTE CARLO PROGRAM FOR X-RAYS DETECTION UP TO 1.4 MeV

Servizio Documentazione
dei Laboratori Nazionali di Frascati

Istituto Nazionale di Fisica Nucleare
Sezione di Torino

INFN/TC-83/2
24 Gennaio 1983

C. Manfredotti and U. Nastasi:

A MONTE CARLO PROGRAM FOR X-RAYS DETECTION UP TO 1.4 MeV

ABSTRACT

A Monte Carlo program has been developed to simulate X-ray spectral response in semiconductor detectors.

Photons in the range from 5 keV to 1.4 MeV are considered as emitted from a source of zero thickness aligned to the crystal axis and followed until their complete energy loss or their escape from the crystal.

The program allows the optimization of important parameters in a semiconductor detector, the study of influence on the spectra obtained and the determination of the energy behaviour of efficiency and energy resolution.

Some obtained results have been compared with experimental data.

1. - INTRODUCTION

Research done in the field of semiconductor detectors has been biased, in recent years, toward detectors made of materials with high and medium atomic numbers[1-8]. The associated wide energy gap allows, in fact, their use at room temperature with no need of cooling to very low temperatures, as is the case with Ge detectors. Furthermore, the high atomic number permits a high detecting efficiency.

At the beginning of the 1970's, mercuric iodide (HgI_2) was shown to be of particular interest in this field; it is a crystal with tetragonal cell structure and a bandgap of 2.1 eV. Its leakage density current at room temperature with an applied voltage of 10^3 volts is of the order of 10-100 pA/cm^2.

Mercuric iodide demonstrates a low mobility both for electrons ($\mu_e = 100$ cm^2/V-sec) and for holes in particular ($\mu_h = 4$ cm^2/V-sec), which is a problem for the transport of charges in the crystal bulk because the trap length of the holes is less than 10^{-1} cm. The crystal must therefore have a thickness of less than 1 mm and a subsequent limitation of the

detectable energy range of up to 1 MeV. The use of such energy excludes the effect of electron-positron pair formation from the incident radiation. Instead, both Compton and Auger photoelectric effects and fluorescence are very important.

This article will describe a Monte Carlo program which, taking into account such phenomena, simulates by a computer the operation of an HgI_2 detector with associated electronics. The use of the program in function of some base parameters like crystal thickness, applied voltage, mobility and so on, permits us to determine their influence upon the detector response. Very important informations can be obtained about the best detecting geometry to use, on the influence of non-uniform electric fields, trapping and processing of signals produced. One can thus establish the optimal dimensions of the crystal and all the necessary parameters which might be useful for the realization of the detector.

2. - COMPUTATIONAL MODEL

Simulating program ISIDE, as previously mentioned, utilizes the well-known Monte Carlo method. Written in FORTRAN, the program is composed of a main part with 40 subroutines with a total of about 1500 statements.

Its running on a VAX 11/780 DIGITAL computer has an average elapsing CPU time from 10 ms for ^{241}Am source with 10^4 generated photons, to 25 ms, for a ^{137}Cs source with 2×10^5 photons. The absence of proportionality between photon number and CPU time is due, as will be seen later, both to the variable detecting efficiency with the photon energy and to the number of Compton events.

ISIDE, which is shown in a block diagram in Fig. 1, can be theoretically divided into four strictly correlated parts: the radiation generation and associated geometry, the energy transfer, carriers transport, and the signal generation and processing. Now let's examine each of the most important parts:

a) Source and geometry

The program simulates a X radiation source of zero thickness and circular shape of which the radius is inserted by the operator with the input data. Cases with a point source can therefore be analized. The source is aligned to the crystal axis, assumed to be cylindrical, and the flight angles of generated photons are randomly chosen within the source-detector solid angle[9].

For each source under consideration a maximum of six photon energies can be emitted taking into account the respective photon percentage with a value between 5 keV and 1.4 MeV. Every single photon is followed until its complete energy loss or its escape from the crystal. Photons which do not enter the active zone (the zone between the two electrodes) are considered lost, so the results discussed here all refer to a highly collimated source-detec

MAIN

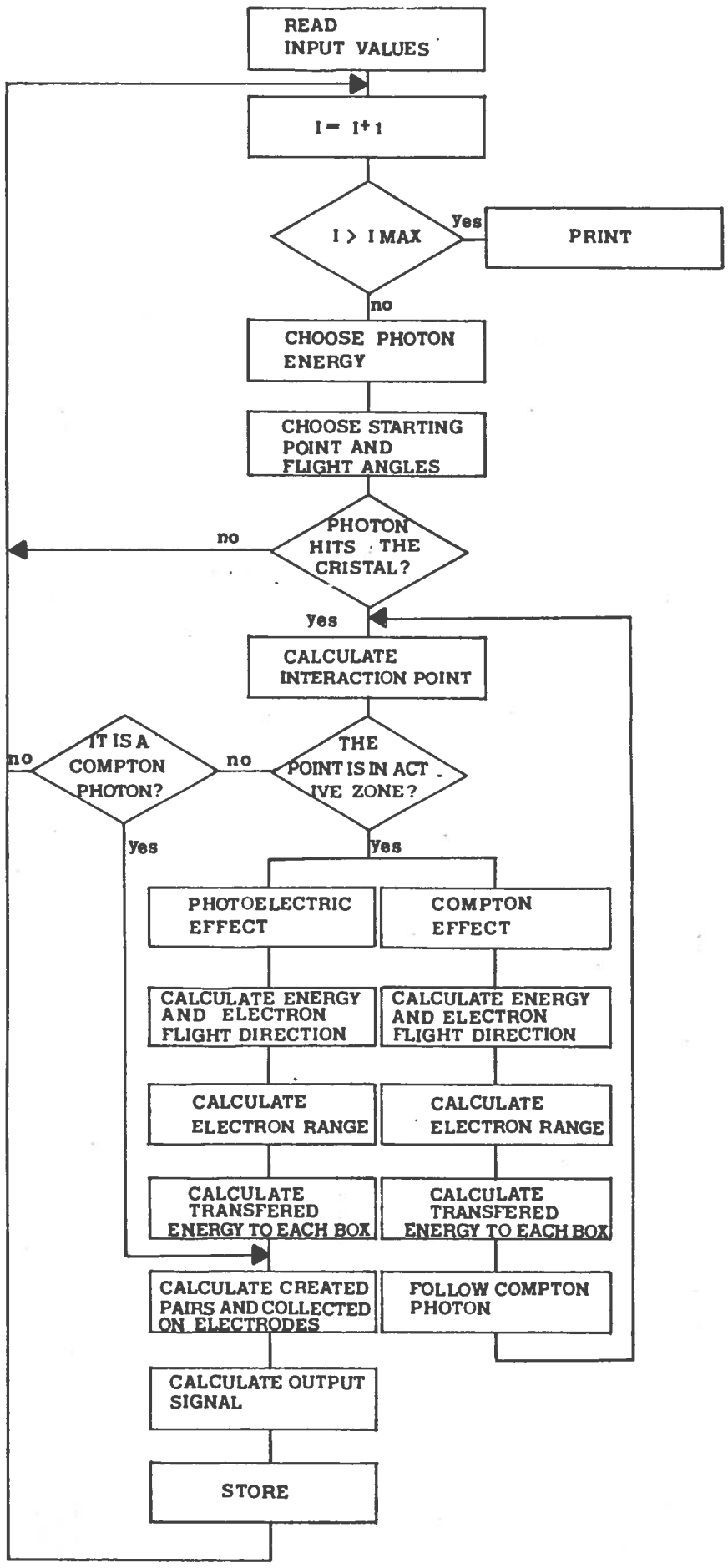

FIG. 1 - Block diagram of the program ISIDE.

tor system.

b) Energy transfer

Inside the crystal, photons cover the length $L = -\ln R/\mu$ where R is a random number between 0 and 1, μ the linear attenuation coefficient of which the values are tabulated[10]. The interaction with matter goes through the two principal phenomena at this energy level: the photoelectric and Compton effects.

In case of photoelectric effect the energy transferred to the electron is $E = h\nu_o - B_e$ where B_e is the electron bound energy and $h\nu_o$ is incident photon energy. For this purpose, the shells K, L1, L2, L3 and an average value of M shell are considered. Flight angles θ for the escaping electron, versus energy, have been computed and tabulated as differential to total cross-section ratio[11]:

$$\frac{d\phi}{\phi} = \frac{3}{4} \frac{\sin^3\theta}{(1 - \beta\cos\theta)^4} d\theta \ ,$$

where $\beta = v/c$; v is the electron speed and c the speed of light. The electron is then followed in the crystal bulk where it loses energy by ionization around its path. The projected range, in mg/cm^2, is determined by the Katz-Penfold formula[12]:

$$Rp = 412\ E^n \ , \qquad n = 1.265 - 0.0954 \ln E \ ,$$

with E as electron energy in MeV.

The average number of e-h generated pairs is $\bar{N} = E/w$ where w is pair creation energy. This value undergoes a Gaussian fluctuation with variance $\sigma = (F\bar{N})^{1/2}$ (with F as the Fano factor), called pair creation noise.

The electron absence in a shell may induce a radiative transition by an electron of the external shells. Since in most cases ($\simeq 80\%$) it is the K shell which is affected by photoelectric effect, the program utilizes the probability ω_K that such a shell will again be filled after a photoelectric event[13,14]:

$$\omega_K = 1/(1 + a_K Z^{-4})$$

with $a_K \simeq 1.12 \times 10^6$.

This procedure allows the observation of the escape peaks K_α in gamma spectrum.

In regards to the Compton scattering, the application of "rejection sampling technique"[15] to the Klein-Nishina cross-section allows us to calculate, with an acceptable CPU time the escaping photon wavelength λ' and, consequently, its scattering angle θ_G :

$$\theta_G = \arccos\left(1 - \frac{m_o c}{h}(\lambda' - \lambda)\right)$$

where m_o is the rest mass of the electron, h the Plank's constant and λ the incident photon wavelength.

The escaping photon energy is:

$$h\nu' = h\nu_o/(1+\alpha(1-\cos\theta_G))$$

where $\alpha = h\nu_o/m_oc^2$.

c) Carriers transport

To analize the generated carriers transport the subroutine DRIFT[16,17,18] has been used. The subroutine considers an applied electric field, of a shape chosen by the operator, which is applied to a crystal of cylindrical shape divided into 50 slabs or "boxes", each with ΔX thickness. The created carriers, under the action of such a field, drift towards the electrodes inducing on them the charge[19]

$$\Delta Q = q\frac{\Delta X\, E(X)}{V}$$

with V the detector voltage, ΔX the slab thickness, E the electric field and q the carrier's charge.

The drift current is influences by the presence of trap levels of the crystal under consideration. The trapped carrier number passing through a ΔX thickness follows a supposed Gaussian distribution with variance $N^{1/2}$ and mean value

$$\Delta N = \frac{N\Delta X}{\mu\tau E(X)}$$

where N is the number of carriers moving in the box, μ the mobility, τ the carrier trapping time. The associated fluctuation is called collection noise. The detrapping is not taken into account because it has a high value compared to the signal formation time.

d) Signal generation and processing

The induced charge vs. time makes a pulse that must be properly filtered and amplified. Time constants of the filters are regulated to maximize the signal noise ratio and such conditions are obtained for $\tau_i = \tau_d$; with τ_i and τ_d the time constants of the integrator and differentiator respectively.

As concerns the electronic noise, it can be obtained from the well-known formula[20]:

$$(\Delta E_N)^2 = (\Delta E_{NO})^2 + (\Delta E_{DE})^2 + (\Delta E_T)^2$$

where the term ΔE_{NO} is the electronic noise of the preamplifier. Generally that is the term which determines the worsening of the energy resolution.

The 2nd term $(\Delta E_{DE})^2$ is proportional to the detector leakage current I_D(pA) :

$(\Delta E_{DE})^2 = 1.18 \times 10^3 I_D \tau$; with τ filters time constant (μsec).

The 3rd term $(\Delta E_T)^2$ depends on the temperature T, on FET preamplifier characteristic, on detector capacity C_D(pF) and on the capacity C_o of the detector-preamplifier connector: $(\Delta E_T)^2 = 0.10\, r_s\, T/\tau\, (C_D^2 + 2C_D C_o)$, where r_s is equivalence series resistance.

In the program we have chosen to insert the electronic noise ΔE_N as input data. This allows us to make optimization tests of such a parameter. The ΔE_N value, inserted by the operator, influences every signal height in a random way according to a Gaussian distribution with variance $\sigma = \Delta E_N / 2.355$.

In conclusion, the signal amplitude is analized and stored in an array which has 121 elements.

3. - COMPUTED RESULTS

In the present study the results are obtained for an HgI_2 crystal. The characteristic of the semiconductor, the source and the detecting system geometry are in Table I.

HD (detector thickness)	$= 5 \times 10^{-2}$ cm
RD (detector radius)	$= 2.56 \times 10^{-1}$ cm
RE (electrodes radius)	$= 2.51 \times 10^{-1}$ cm
H (source-detector distance)	= 10 cm
RS (source radius)	$= 10^{-3}$ cm
FANO (Fano factor)	$= 5 \times 10^{-1}$
KEVP (pair creation energy)	$= 4.15 \times 10^{-3}$ keV
UE (electron mobility)	$= 10^2$ cm^2/V-SEC
TE (electron Trapping Time)	$= 5 \times 10^{-6}$ SEC
UH (hole mobility)	$= 4$ cm^2/V-SEC
TH (hole Trapping Time)	$= 7.5 \times 10^{-7}$ SEC
DENS (density)	$= 6.4$ g/cm^3
TCI (integration time constant)	$= 4 \times 10^{-6}$ SEC
TCD (differentiation time constant)	$= 4 \times 10^{-6}$ SEC
V (total detector voltage)	= 1500 VOLTS
PS(1) - PS(6) (gamma probabilities	
ES(1) - ES(6) (gamma energies	
P(8, 9) (photoelectric flight angles cumulated probabilities)	
BE(2, 4) (electron binding energy in K and L shell)	
ENOISE (electronic noise)	

TABLE I - Input data of program ISIDE. If not differently specified, these values were used in the program.

The obtained detector efficiency for a crystal of 500 μm thickness and defined as (interacting photons number)/(incident photons number) is shown in Fig. 2. It can be noted that it strongly diminishes for energy greater than 60 keV reaching the 1 % value at 1 MeV. Fig. 3 shows the photopeak efficiency i. e. (number of photons that undergo photoelectric effect)/(number of incident photons), versus energy. The simulation program can consider photons incident on cathode (direct bias) and incident on anode (reverse bias). In both cases, we may obtain the collection efficiency reported in Fig. 4 and defined as (number of carriers collected on the electrodes)/(number of generated carriers in the crystal). It can be seen

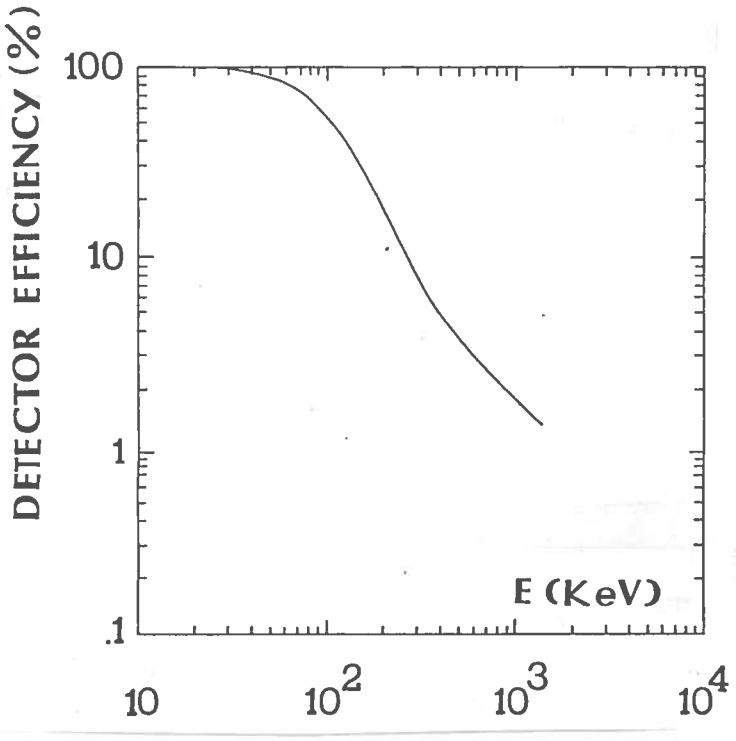

FIG. 2 - Theoretical detector efficiency values as a function of radiation energy E.

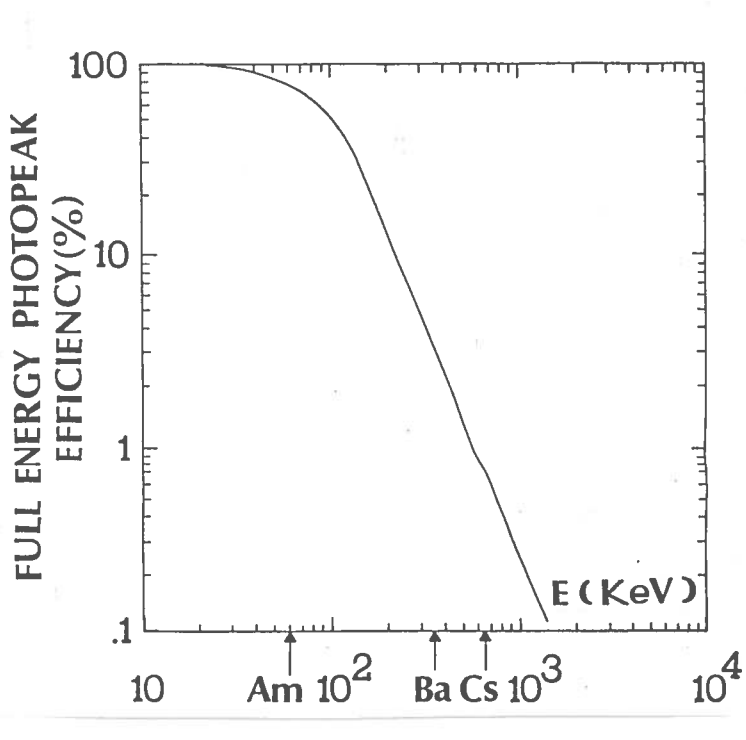

FIG. 3 - Theoretical full energy photopeak efficiency values as a function of radiation energy E.

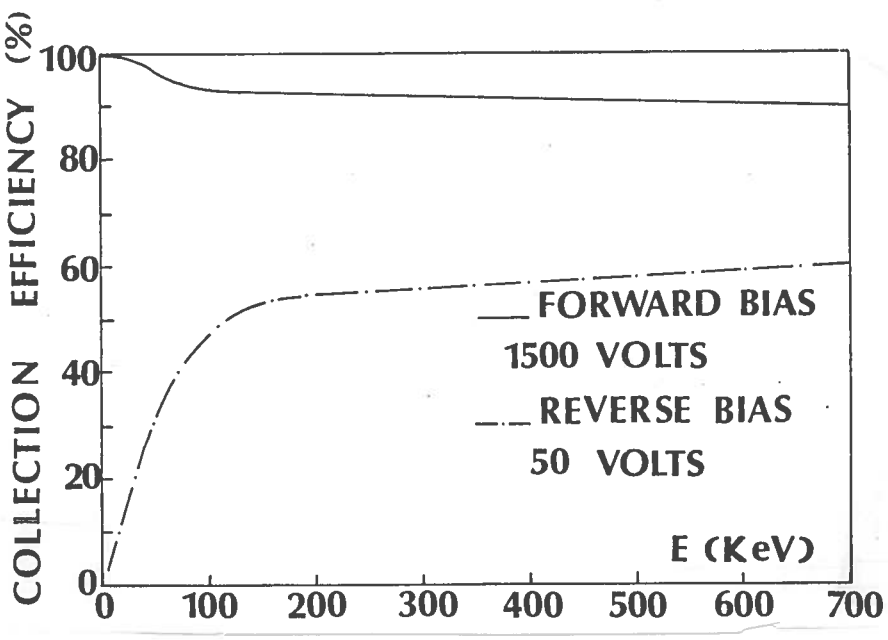

FIG. 4 - Theoretical collection efficiency values as a function of radiation energy E.

that the collection efficiency, with an applied voltage of 1500 volts in the case of direct bias, energy increase diminishes and is stabilized after only 100 keV, thus becoming independent of the energy of incident photons. This occurs because the holes are generated in the proximity of the negative electrode and are immediately collected, contributing actively to the formation of output pulses. At high energy values, on the contrary, these are created in the proximity of the positive electrode and must therefore cross the crystal to reach the cathode, while the electrons are collected instantaneously. The second curve has been obtained in a case of reverse bias of 50 volts. Thus, as we expected, the collection efficiency improves with the energy increase, for the same reasons discussed before.

Figs. 5, 6 and 7 present the simulated spectra of a source ^{137}Cs for three different values of $(\mu\tau)_h$ product ($\mu\tau$ for electrons is kept constant and equal to 5×10^{-4} cm^2V^{-1}). The $(\mu\tau)_h$ value closest to the experimental spectrum[10] (see Fig. 8) is about $2\text{-}5 \times 10^{-6}$ cm^2V^{-1}. Note that the second peak is a K (Hg) escape peak, while the tail at lower energies is due to Compton effect.

In Fig. 9 we find a simulated spectrum of ^{241}Am source. Compton effect is nearly absent, thus permitting a clear view of the peaks. There is no background because, as has already been stated, the electronic noise is considered to be only the fluctuation of the

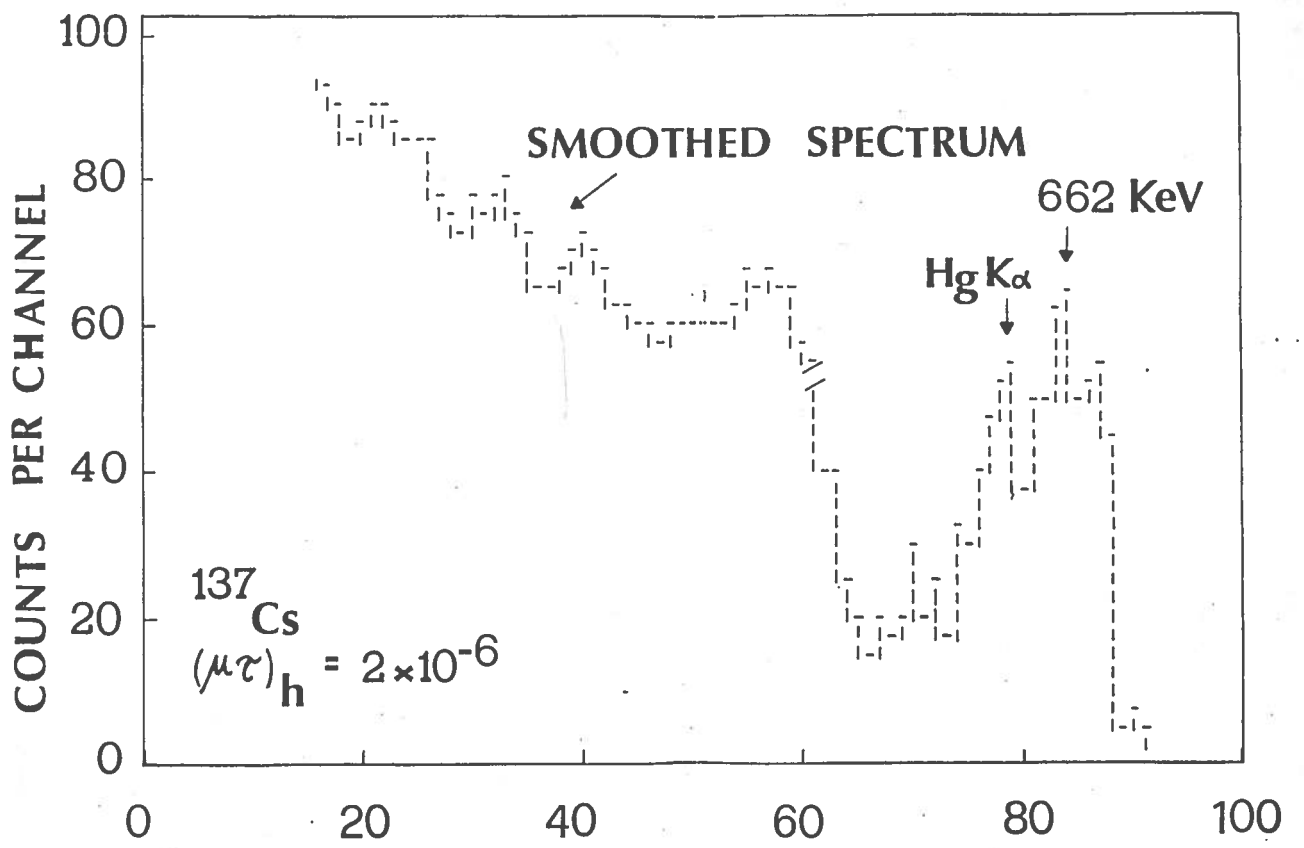

FIG. 5 - Simulated ^{137}Cs spectra: $(\mu\tau)_e = 5 \times 10^{-4}$ and $(\mu\tau)_h = 2 \times 10^{-6}$.

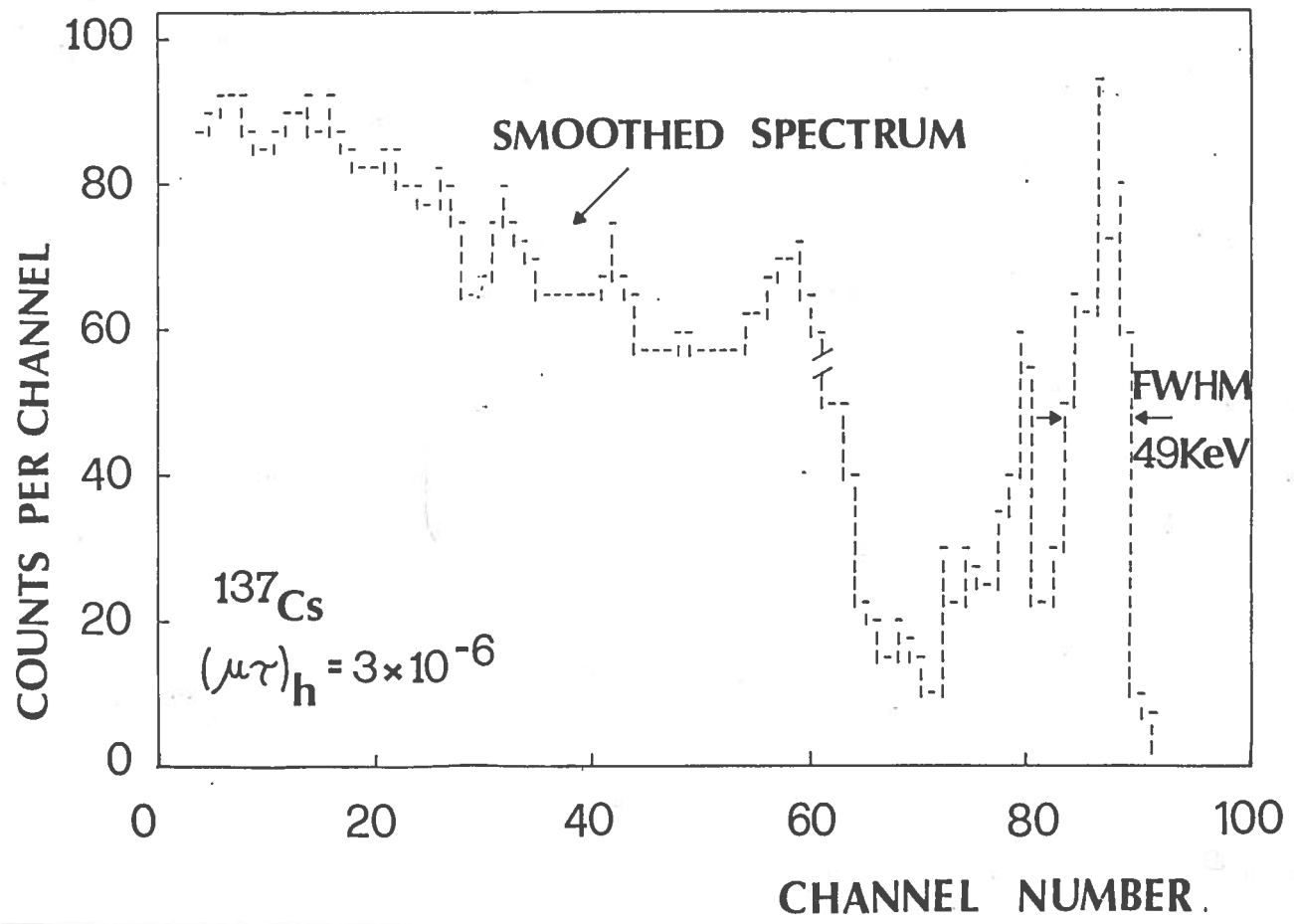

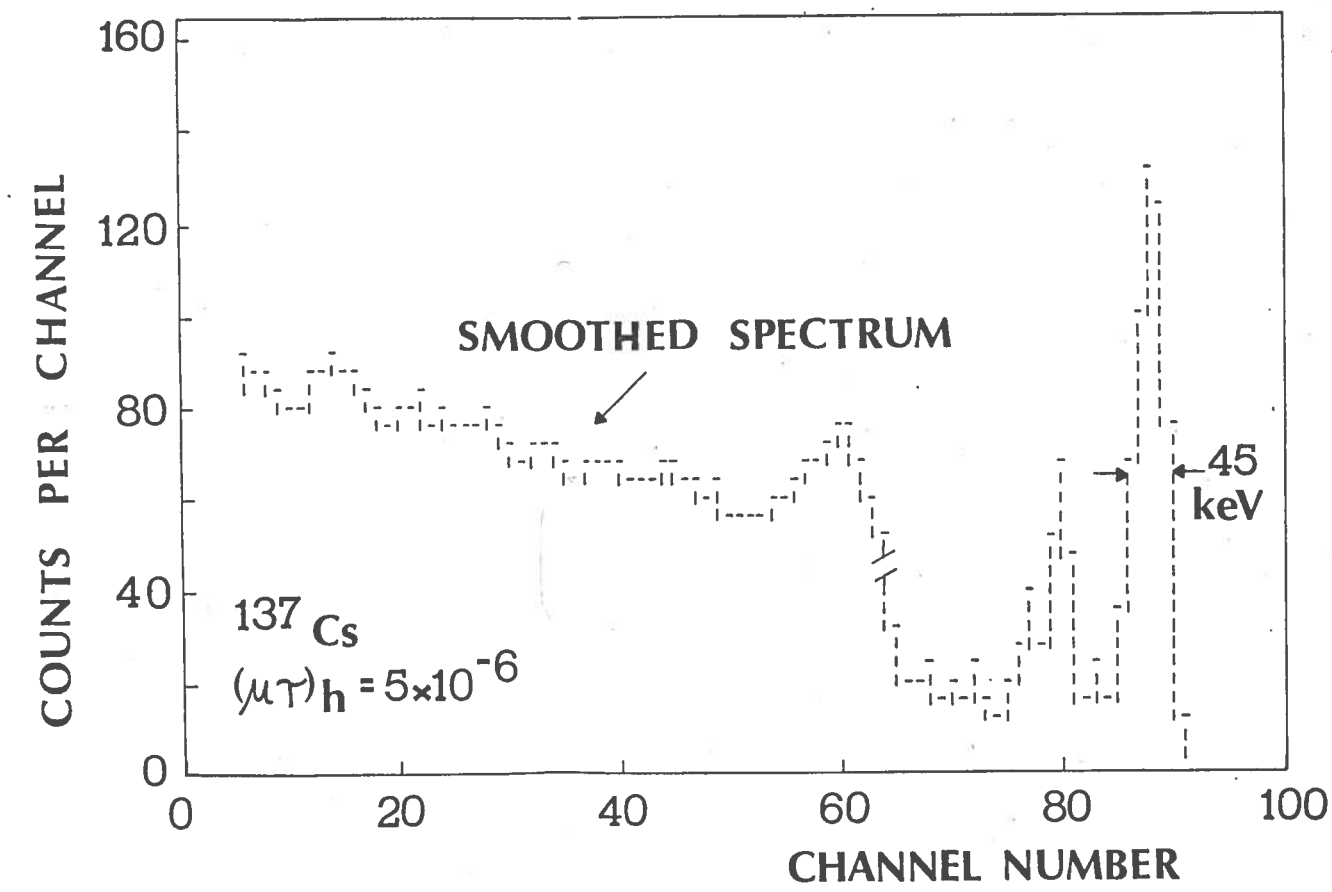

FIG. 6 and 7 - Simulated ^{137}Cs spectra: $(\mu\tau)_e$ is constant and $(\mu\tau)_h$ is varying according to indicated values.

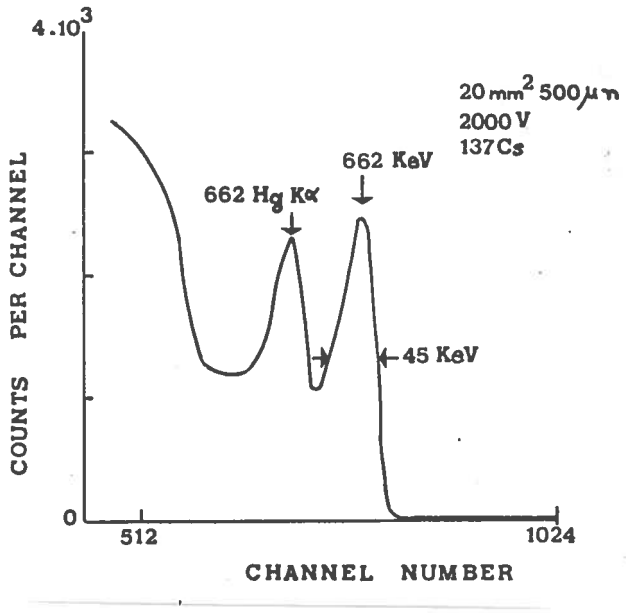

FIG. 8 - An example of experimental ^{137}Cs spectrum.

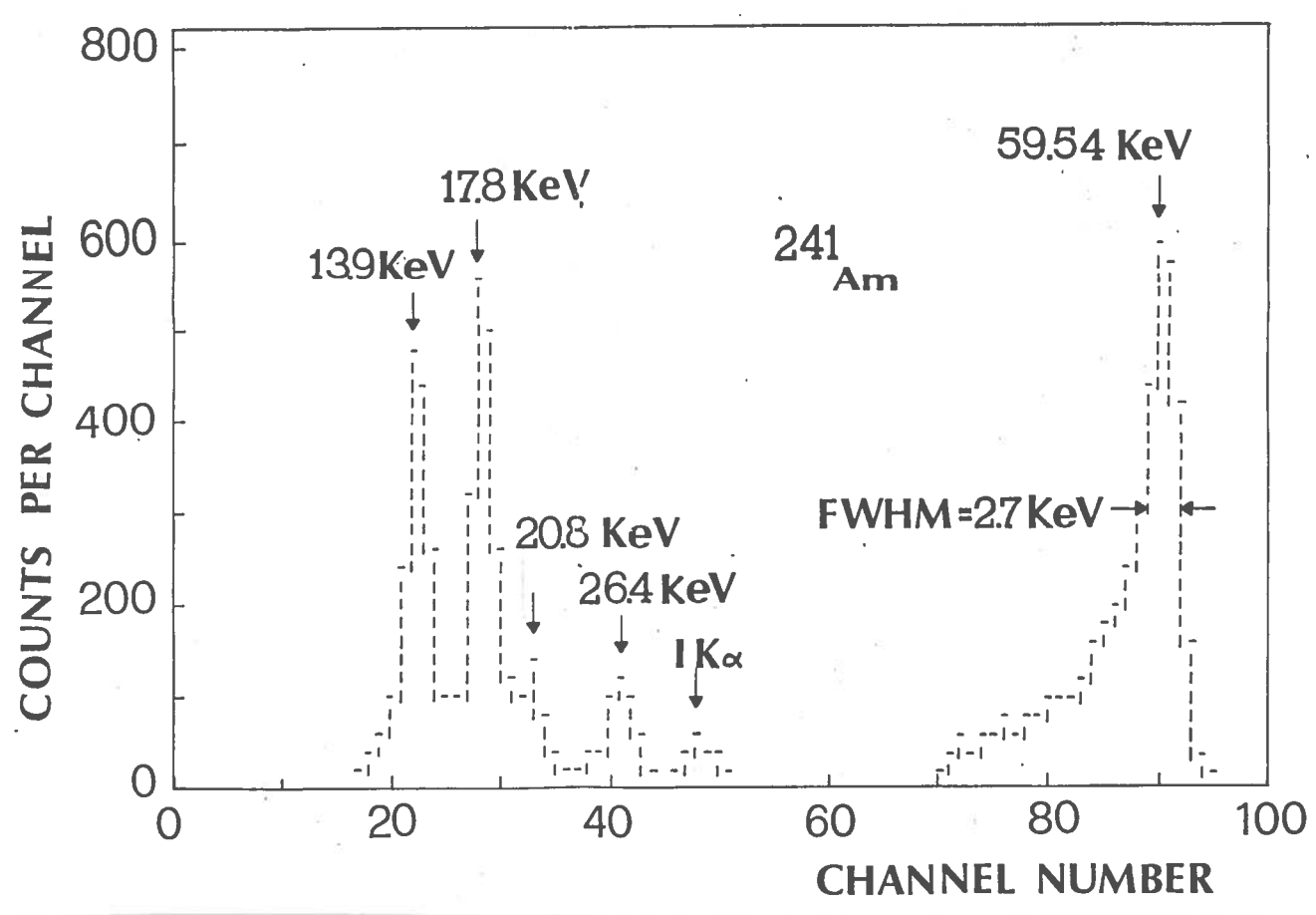

FIG. 9 - Simulated ^{241}Am spectrum.

signals emerging from the detector. To the left of the photoelectric peak, we can clearly see a tail which is due to the trapping of the carriers. The resolution at 60 keV is $\simeq$2.7 keV (4.4%).

In Figs. 10 and 11 on the other part, simulated spectra of ^{241}Am and ^{137}Cs sources are reported, which are obtained through reversal of the voltage polarity on the crystal. The reverse bias, by lowering the hole collection efficiency, influences more strongly the ^{241}Am spectrum than the ^{137}Cs spectrum, which is affected only by the low value of the bias.

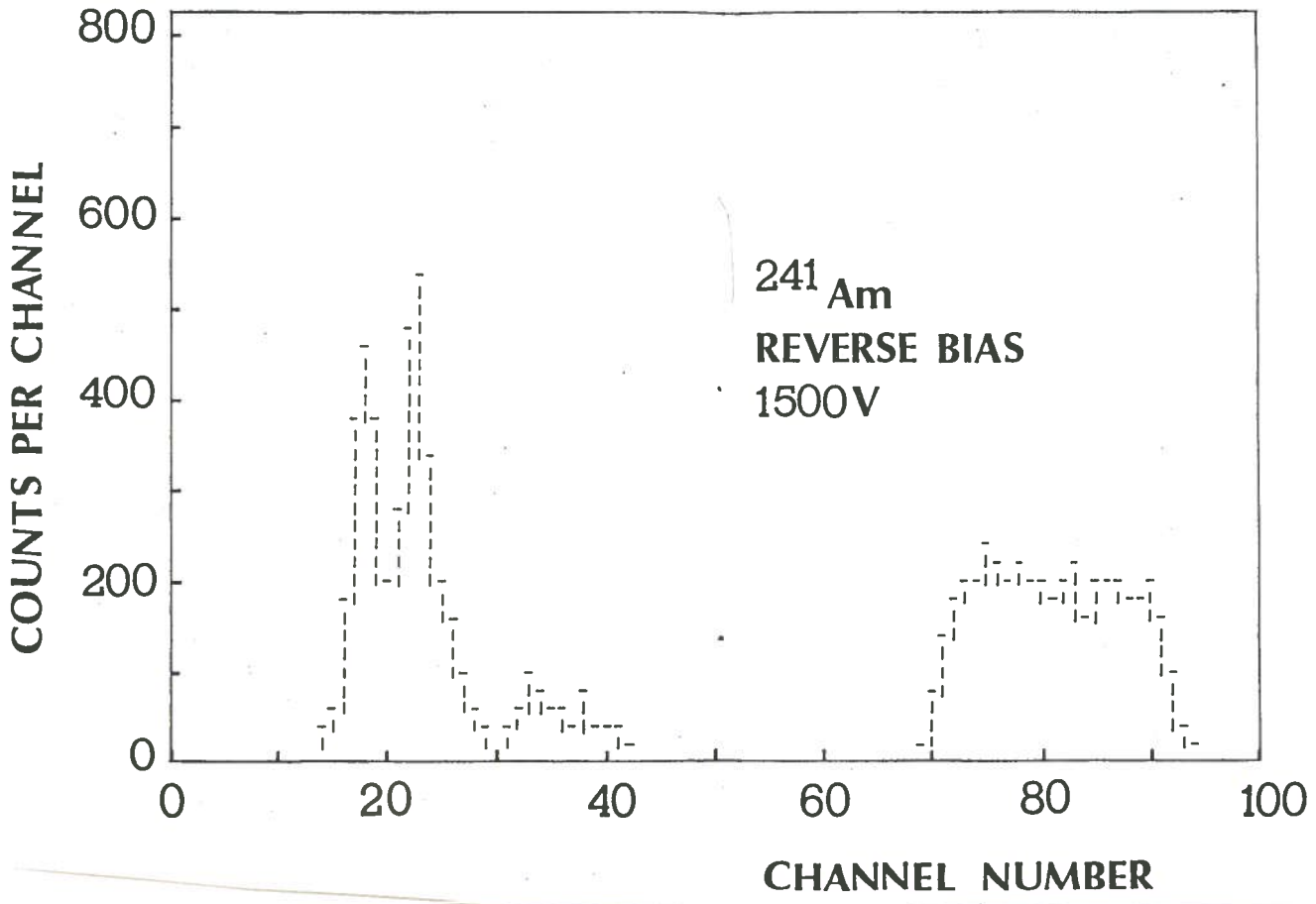

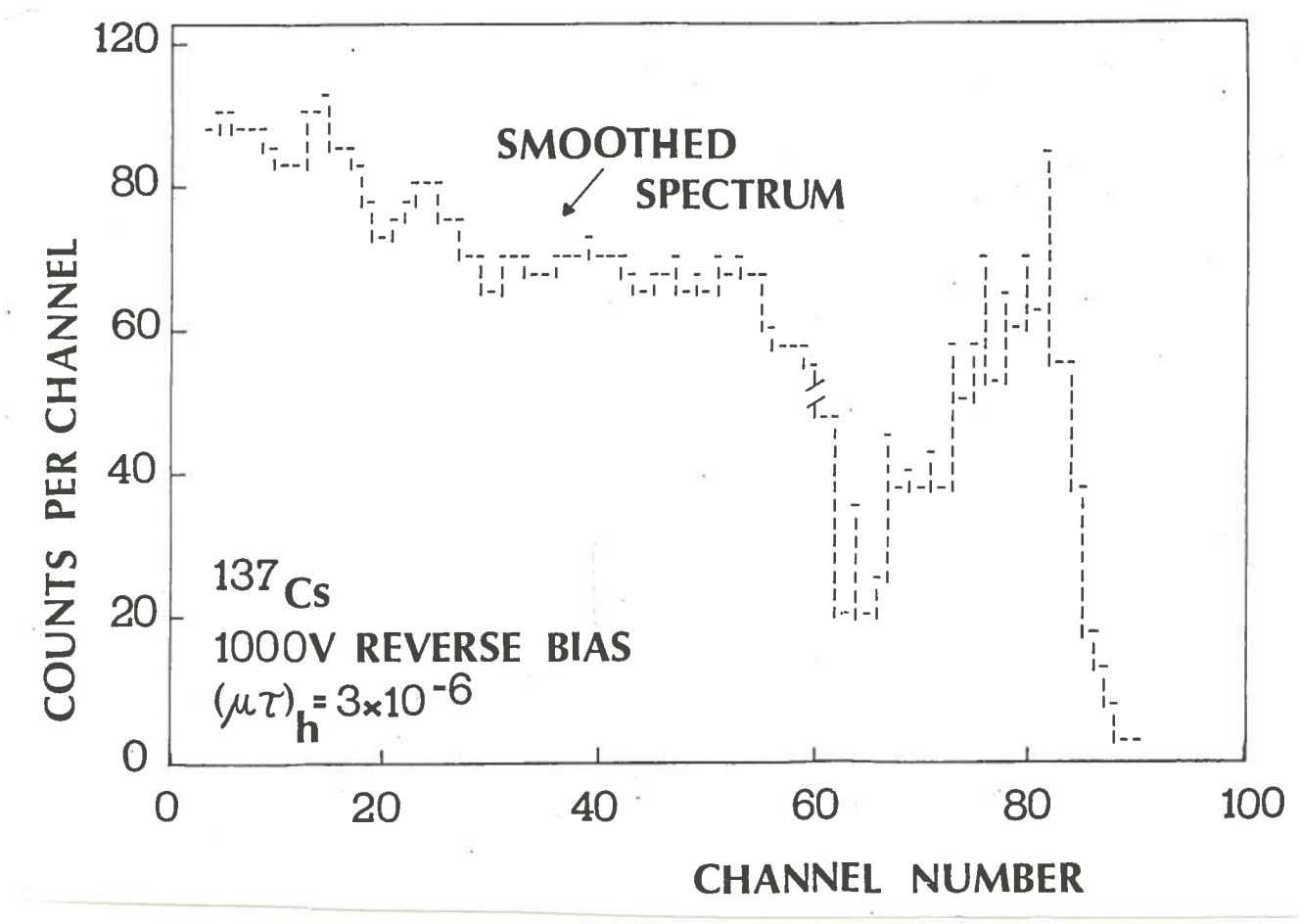

FIG. 10 and 11 - Simulated spectra of ^{241}Am and ^{137}Cs with gammas incident on the anode.

The spectra of Figs. 12, 13, 14 and 15 were obtained with a source of ^{57}Co with a variable applied voltage and, therefore, a variable trapping length of the carriers. It has been seen that the tails to the left of the photoelectric peaks diminish when voltage is increased with a notable improvement in the resolution of the peaks themselves.

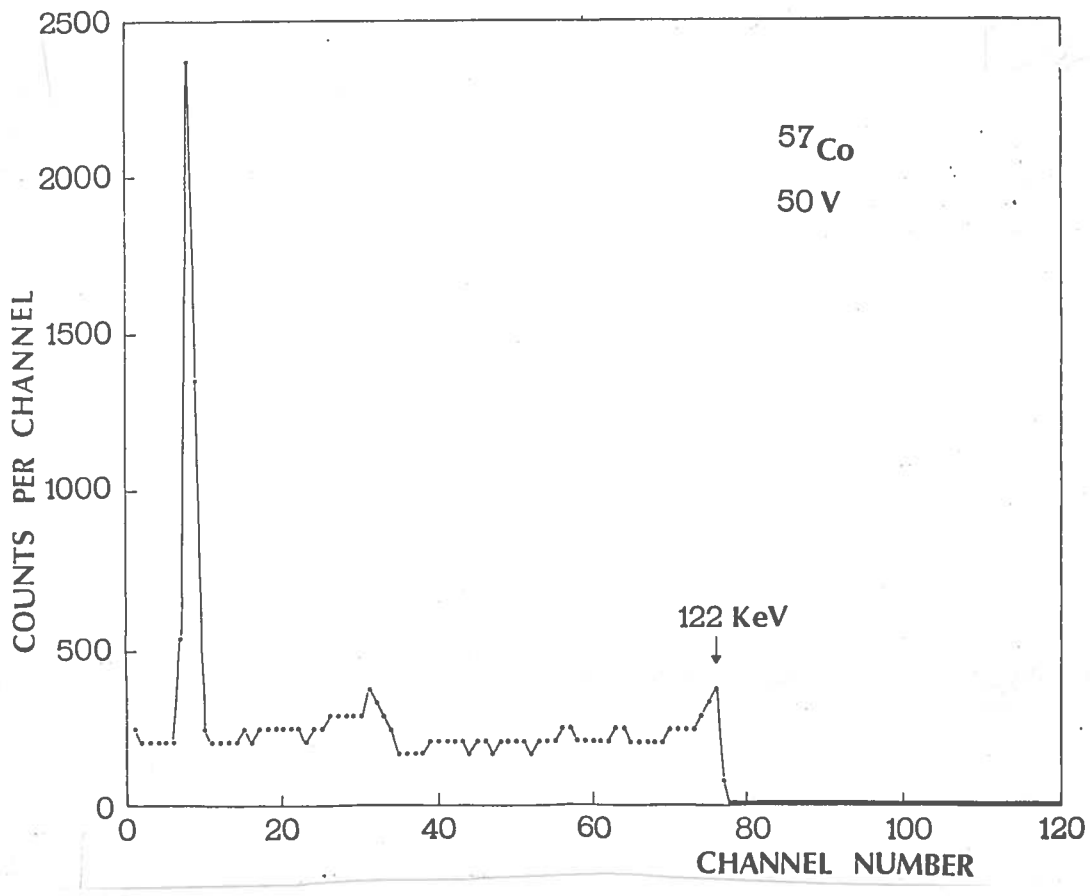

FIG. 12

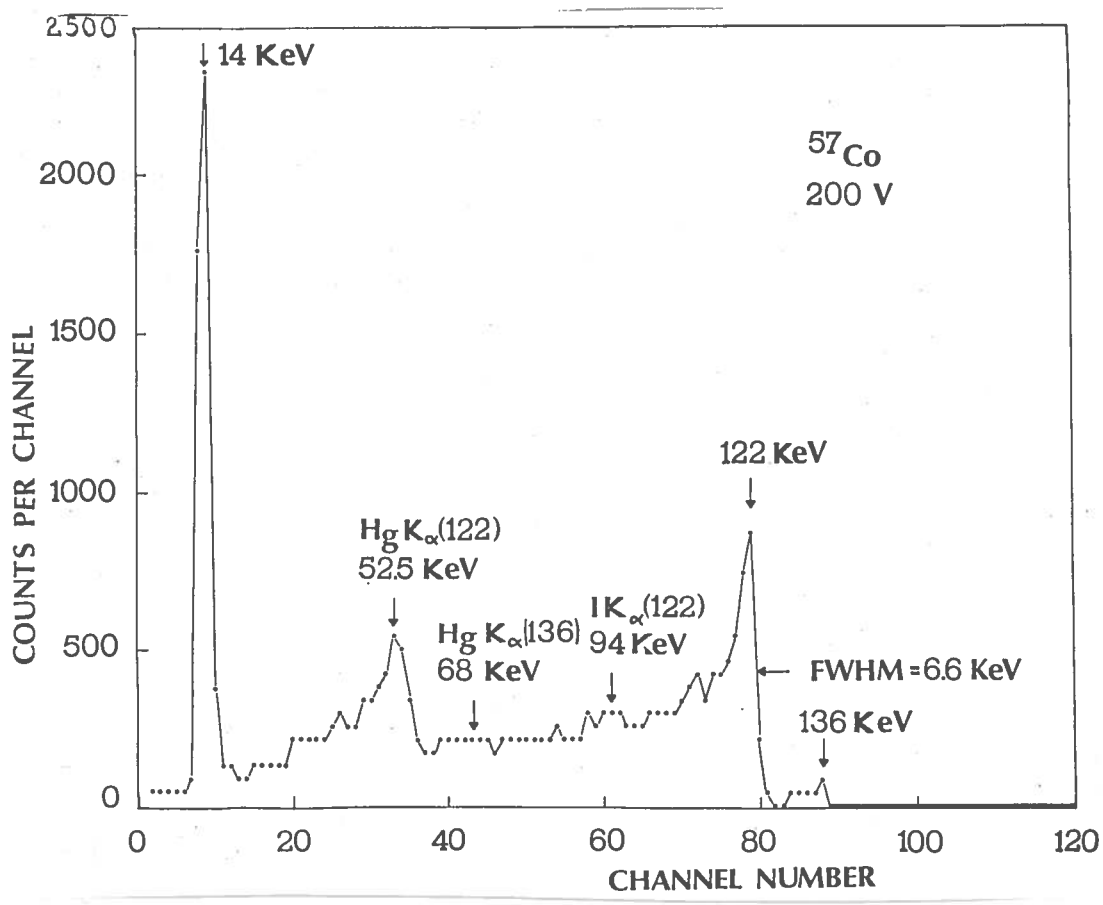

FIG. 13

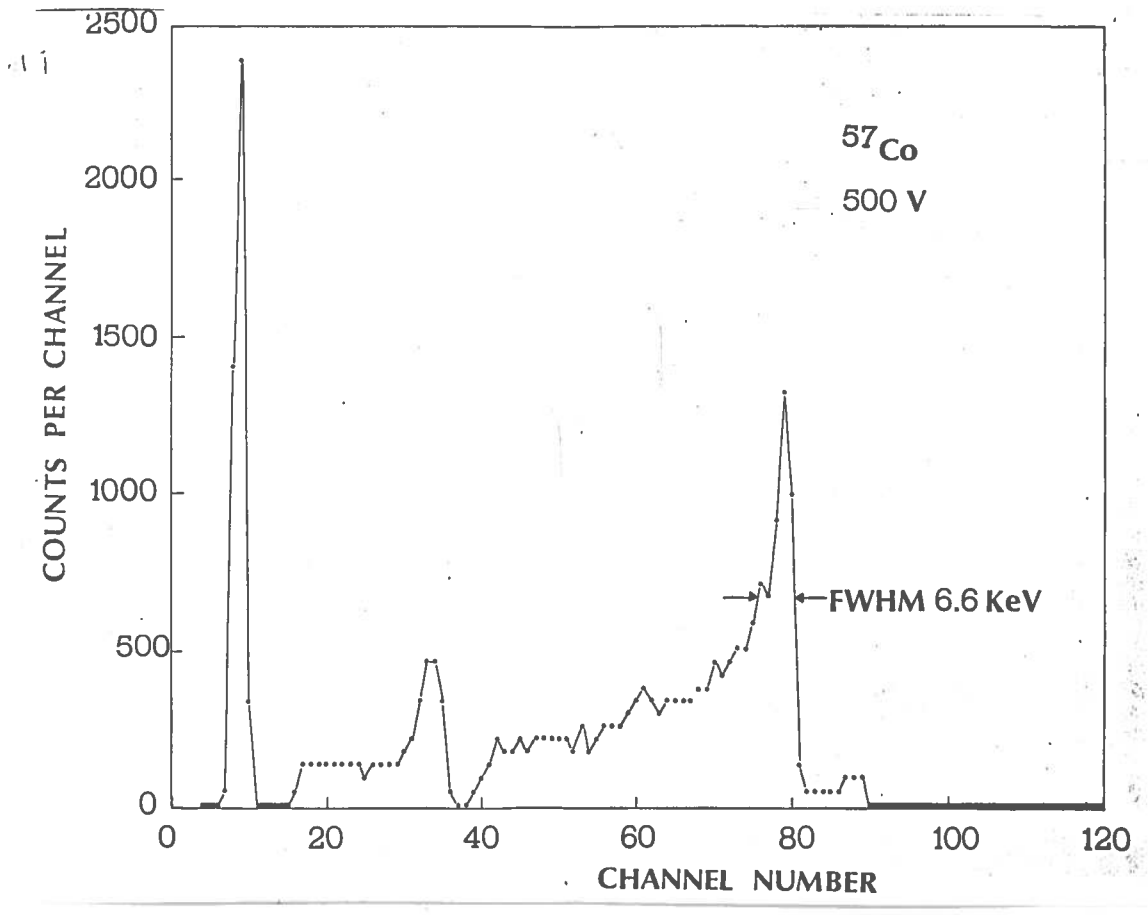

FIG. 14

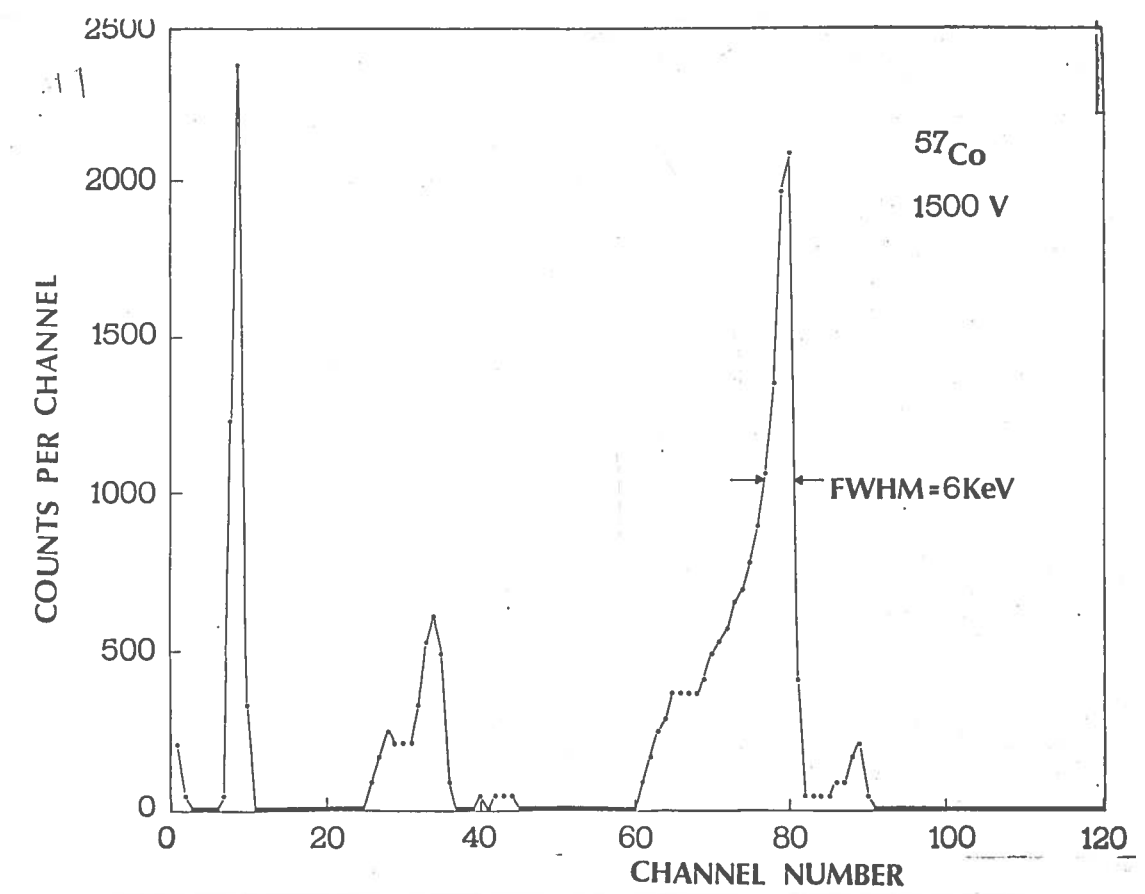

FIG. 15

FIG. 12, 13, 14 and 15 - Evolution of ^{57}Co spectrum as a function of the detector voltage.

Fig. 16 shows the energy resolution (FWHM) of the detector as a function of gamma energy; a sharp increase in FWHM above 300 keV is clearly evident. The agreement with average data quoted in the literature in this field[21] is reasonable, taking into account likely differences in crystal quality.

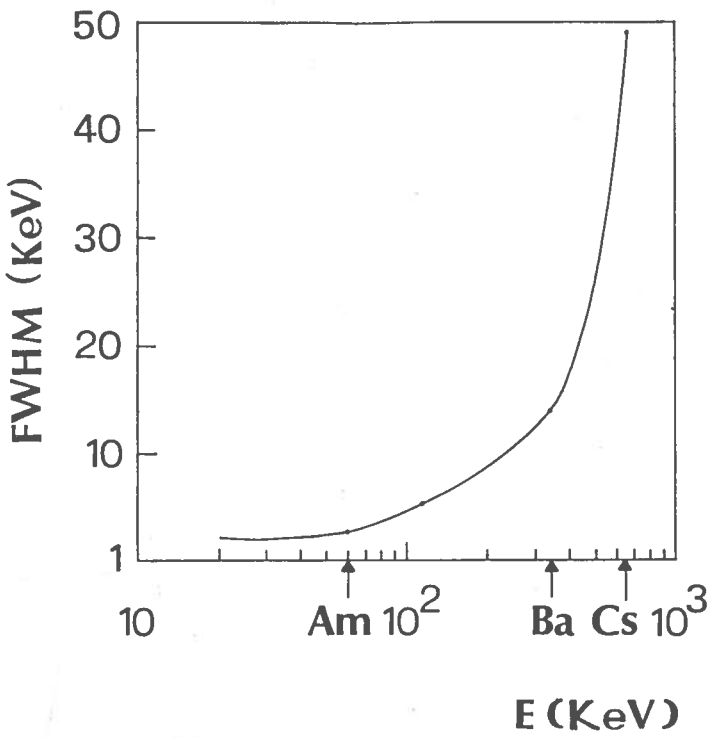

FIG. 16 - Energy resolution of the detector expressed as full width at halh maximum (FWHM) as a function of radiation energy.

Finally, Fig. 17 reports a representation in a Gaussian scale of ^{241}Am and ^{57}Co photoelectric peaks. The absence of linearity in the low energy side is clearly due to trapping effects. Also in this case, the similarity with experimental behaviours[21] is rather strong.

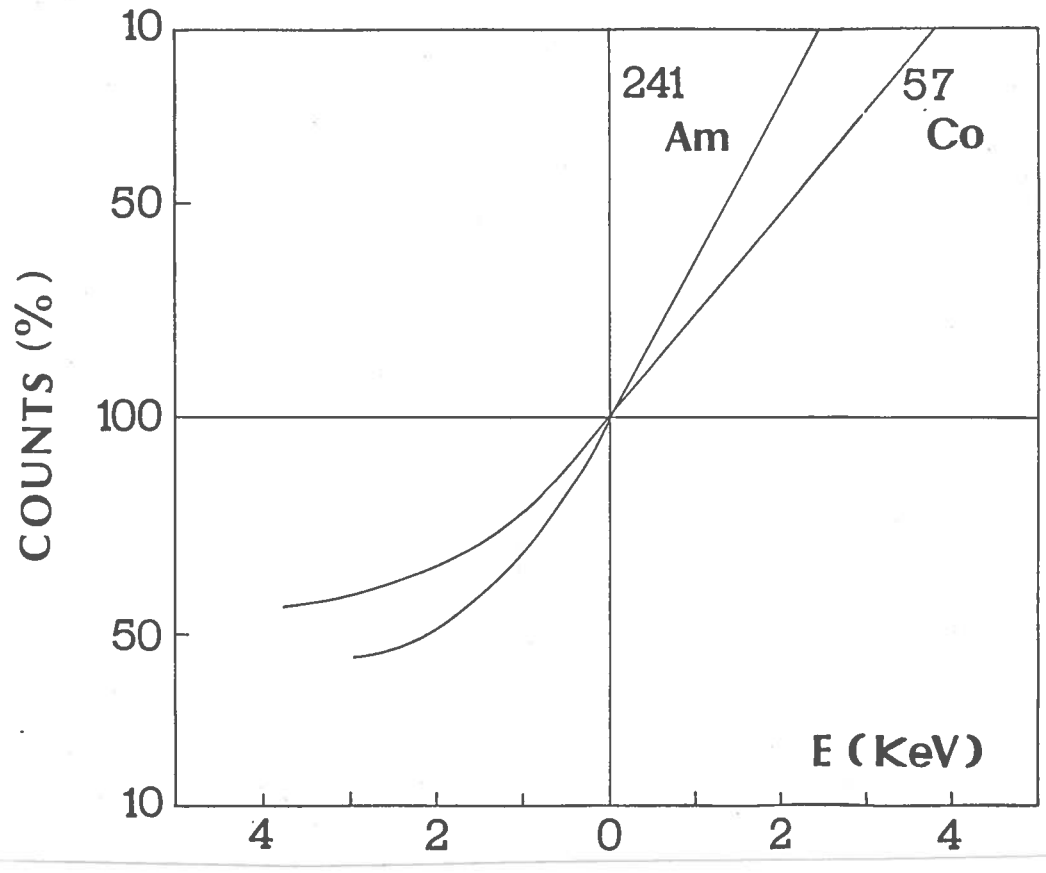

FIG. 17 - Shapes of the photoelectric peaks of ^{241}Am (59.5 KeV) and ^{57}Co (122 KeV) reported in a Gaussian scale.

4. - CONCLUSIONS

This study shows that the Monte Carlo method is a reliable and powerful technique which allows us to forecast detector performances very quickly and in great detail.

The agreement with experimental data indicates that the various phenomena occuring in the crystal are taken into account in the right way. The part relative to signal generation and treatment can be adapted to the various possible experimental conditions. Future studies will investigate in detail the possibilities of the Monte Carlo method used for a detector optimization and various physical effects which are at present not completely understood or neglected (polarization, dependnece of τ on the electrical field, etc.).

(*) The program in FORTRAN IV version for a VAX 11/780 DEC computer is available. Please contact Dr. U. Nastasi, Istituto di Fisica Superiore, Torino (Italy).

REFERENCES

(1) - H. L. Malm, IEE Trans. Nucl. Sci., NS-19, 263 (1972).

(2) - H. L. Malm, T. W. Raudolf, M. Martini and K. R. Zanio, IEE Trans. Nucl. Sci., NS-20, 500 (1973).

(3) - S. P. Swierkowski, G. A. Armantrout and R. Wichner, Appl. Phys. Letters, 22, no. 5, 281 (1973)

(4) - R. O. Bell, F. V. Wald, C. Canali, F. Nava and G. Ottaviani, IEE Trans. Nucl. Sci., NS-21, 331 (1974).

(5) - H. L. Malm and M. Martini, IEE Trans. Nucl. Sci., NS-21, 332 (1974).

(6) - S. P. Swierkowski, G. A. Armantrout and R. Wichner, IEE Trans. Nucl. Sci., NS-21, 302 (1974).

(7) - J. Llacer, M. K. Watt, M. Schieber, R. Carlston and W. Schnepple, IEE Trans. Nucl. Sci. NS-21, 305 (1974).

(8) - J. P. Ponpon, R. Stuck, P. Siffert and C. Schwab, Nuclear Instr. and Meth. 119, 197 (1974).

(9) - M. Belluscio, R. De Leo, A. Pantaleo and A. Vox, Nuclear Instr. and Meth. 118, 553 (1974).

(10) - M. Schieber, I. Beinglass, G. Dishon and A. Holzer, Mercurie iodide nuclear detectors, School of Applied Science and Technology, the Hebrew University, Jerusalem (Israel).

(11) - W. Heitler, The Quantum Theory of Radiation, 3rd ed. (Oxford Univ. Press, 1974).

(12) - L. Katz and A. S. Penfold, Rev. Mod. Phys. 24, 28 (1952).

(13) - E. H. S. Burshop, The Auger Effect and other Radiationless Transition (Cambridge Univ. Press).

(14) - J. R. Greening, Fundamental of Radiation Dosimetry, Medical Physics Handbooks.

(15) - D. E. Raeside, Phys. Med. Biol. 21, 181 (1976).

(16) - G. A. Armantrout and C. Manfredotti, private communication.

(17) - S. P. Swierkowski and G. A. Armantrout, IEE Trans. Nucl. Sci. NS-22, 205 (1975).

(18) - S. P. Swierkowski, IEE Trans. Nucl. Sci. NS-23, 131 (1976).

(19) - G. Bertolini and A. Coche, Semiconductor Detectors (North-Holland, 1968).

(20) - M. Slapa, G. C. Hunt, W. Seibt, M. Schieber and P. Randte, IEE Trans. Nucl. Sci. NS-23, 102 (1976).

(21) - C. Scharanger, P. Siffert, A. Holzer and M. Schieber, IEE Trans. Nucl. Sci. NS-27, 276 (1980).